SAND2017-2228J

Alignment, Dissociation and Ionization of the H_2 Molecule in Intense Laser Fields Using Velocity Mapped Imaging

Gary V. Lopez[a], Martin Fournier[a], Justin Jankunas[a], Alexandros K. Spiliotis, T. Peter Rakitzis[b] and David W. Chandler[a]*

[a]*Combustion Research Facility, Sandia National Laboratories, Livermore, California 94550*

[b]*Department of Physics, University of Crete, and Institute of Electronic Structure and Laser, Foundation for Research and Technology-Hellas, Heraklion-Crete, Greece*

Abstract

Alignment, dissociation and ionization of H_2 molecules in the ground or the electronically excited E,F state of the H_2 molecule are studied and contrasted using the Velocity Mapping Imaging (VMI) technique. Photoelectron images from non-resonant 7-, 8- and 9-photon radiation ionization of H_2 show that the intense laser fields create ponderomotive shifts in the potential energy surfaces and distort the velocity of the emitted electrons that are produced from ionization. Photofragment images of H^+ due to the dissociation mechanism that follows the 2-photon excitation into the (E,F; ν = 0, J = 0, 1) electronic state show a strong dependence on laser intensity, which is attributed to the high polarizability of the H_2 (E,F) state. For transitions from the J = 0 state, particularly, we observe marked structure in the angular distribution, which we explain as the interference between the prepared J = 0 and Stark-mixed J = 2 rovibrational states of H_2, as the laser intensity increases. Quantification of these effects allows us to extract the molecular polarizability of the H_2 (E,F) state, and yields a value of 103 $\pm$ 37 A.U.

*Corresponding Author: chand@sandia.gov

I. Intoduction

Like atoms, molecules can absorb many non-resonant photons from an intense laser radiation field and ionize; and processes such as above threshold ionization can be observed.[1] However, molecules also possess dissociative pathways as well as ionization pathways. Phenomena such as dissociative ionization[2] and multiphoton ionization[3] are easily observed in most small molecules and by studying these processes one can learn about the details of the nature of the molecular bonding, electron distributions and couplings between different electronic states.

Molecular hydrogen is one of the most abundant materials in the universe and despite being the simplest and most studied neutral molecule it remains a great challenge for theory when coupled to intense laser fields.[4] Many exquisitely precise experimental studies and extensive quantum chemical calculations have been performed on isolated molecular H_2 but with the advent of more and more intense laser sources, the interest on dissociation and ionization processes of molecular hydrogen and deuterium has increased in the last decades.[1-33] In this study, we utilize laser intensities between 5×10^{10} W/cm^2 and 2×10^{14} W/cm^2.

A resonant multiphoton ionization process in molecular hydrogen that has received much attention in the last two decades involves the two-photon excitation to the E,F $^1\Sigma_g^+$ state followed by subsequent absorption of one photon to cause ionization.[28-30] The unusual shape of the E,F electronic potential curve has two minima resulting from the avoided crossing of the $(1s\sigma_g)$ $(2s\sigma_g)$, E state, and $(2p\sigma_u)^2$, F state, potential energy curves. It is expected that the double-minimum nature of this intermediate state should manifest itself in several ways in the ionization due to the homogeneous perturbations between vibronic levels associated with the ionic inner (E state) and covalent outer (F state) wells and the expected large variation of the transition moment with H-H internuclear distance.[29] The resonant 2+1 process is conveniently employed to determine internal-state populations of H_2 in molecular dynamics experiments involving gas-phase and gas-surface scattering as stated in previous studies.[13, 28, 29, 34-37] We utilize the two-photon excitation to populate a particular rotational state of the E,F state from which to perform 532 nm non resonant dissociation and ionization studies.

The ion-imaging technique was first demonstrated by Chandler and Houston[38] to record spatial distributions of photodissociation products. Higher resolution was

achieved by Eppink and Parker[39] utilizing an ion lens in the detection path, this transformed the image from a spatial image to a velocity image (Velocity Mapping), improving the resolution of the velocity measurement. This technique has become a standard method in the study of molecular photodissociation and bimolecular scattering.[40-49]

In the present study, we utilize the Velocity Mapped Imaging technique to study the intensity dependence of the angular distributions of H^+ production channels associated with either ionization of $H_2(X)$ followed by dissociation with 532-nm laser light, or dissociation of $H_2(E,F;\ \nu = 0,\ J = 0, 1)$ followed by ionization of the $H(N = 3)$ atom fragment. By quantification of the angular distributions as a function of laser intensity, we learn about the mechanisms that generate the H^+ (Fig. 1) as well as measure the molecular polarizability of the E,F state of H_2 for the first time. Ponderomotive shifts in the potential energy surfaces and hence distortions in the velocity of the emitted electrons that are produced from 7-, 8- and 9-photon ionization caused by intense laser fields were observed from the non-resonant 532 nm laser radiation ionization of H_2. The recorded photoelectron images are found to arise from H_2^+ that is highly aligned with the 532-nm laser polarization. The laser does not however align the $H_2(X)$ ground state but selects those molecules whose internuclear axes are aligned with the laser beam polarization axis. Because of this selectivity the photoelectron images reveal the molecular frame photoelectron spectra.

II. Experimental Method

A. Non-resonant 532-nm photodissociation of ground state H_2

A skimmed molecular beam of 10% H_2 (Matheson gas purity > 99.99%) diluted in He, in order to minimize space-charge distortions due to producing too many ions with a single laser shot, is crossed by a beam of 532-nm laser light (Fig. 2). The gas is delivered through a pulsed valve (30-psi backing pressure) with a 20-μs pulse width Amsterdam Cantilever Piezo Valve and skimmed by a 3-mm diameter skimmer (Beam Dynamics). A 108-ps pulse length stimulated Brillouin scattering (SBS) compressed high energy Nd:YAG laser (SL330 – EKSPLA) was used in these experiments. The laser beam is focused with a 178 mm fused silica lens onto the molecular beam (also shown in Fig. 2). Our ion optics was calibrated with the non-resonant 532 nm photoelectron image of Kr.

B. 532-nm dissociation following 2-photon excitation of H_2 (E,F; $\nu = 0$, $J = 0, 1$)

Individual (E,F $^1\Sigma_g^+$) rovibronic levels of H_2 are populated by tunable, pulsed ultraviolet laser radiation. This laser radiation is generated by propagating the visible output of the Sirah PrecisonScan dye laser (Mix Rhodamine 610 + Rhodamine 640 in methanol dye, $\lambda =$ 598 - 636 nm, bandwidth = 0.04 cm^{-1}) through a frequency-doubling, a frequency-tripling and tracking units containing KDP and BBO crystals. Photofragment images of H^+ following 532 nm irradiation of the H_2 (E,F; $\nu = 0$, $J = 0$) and H_2 (E,F; $\nu = 0$, $J = 1$) state were recorded. The H_2 (E,F; $\nu = 0$, $J = 0, 1$) levels were populated by the 2-photon excitation of ground state H_2 at 201.683 nm and 201.796 nm, respectively. Two different lasers are used to perform these experiments: a single-mode (Coherent "Infinity") laser system having a 4 ns pulse length or a 108 ps pulse length stimulated Brillouin scattering (SBS) compressed high energy Nd:YAG laser (SL330 – EKSPLA). The laser beams are focused with a 220 mm fused silica lens onto the molecular beam. In these experiments a molecular beam of neat H_2 (Matheson gas purity > 99.99%) is utilized.

C. The velocity-map imaging lens and the electron/fragment detection system

The photodetached electrons or H^+ fragments are accelerated towards a position-sensitive detector consisting of a set of 75 mm diameter micro-channel plates (MCP) coupled to a phosphor screen (Photonis USA, Inc) and a charge-coupled device (CCD) camera (Andor's Zyla 5.5 sCMOS camera, 2560 × 2160 pixels). The imaging detector is located at the end of the VMI spectrometer (Fig. 2). The VMI lens and the entire electron flight path are enclosed within a concentric cylinder of μ - metal shielding (0.76 mm thick, 13.2 cm diameter, 84 cm length). There are four holes (3 cm diameter) equally spaced each 90 degrees around the perimeter, located 5 cm from one end of the tube. Velocitas VMI DOUBLE PRIME ion optics are utilized in these experiments.

III. Theoretical Method

The effect of molecular polarizability on a molecule with no permanent dipole moment, subject to an electric field, was studied by Friedrich and Herschbach.[50] Intense laser fields on polarizable molecules tend to distort the electronic distribution

of the molecule, thus inducing a dipole moment. The interaction potential of this process is governed by a $\cos^2\theta$ distribution. As a result, aligned pendular states are created, which are superpositions of the field-free rotational states. For sufficiently intense fields, the angular distribution of the molecular alignment is distorted, and the structure that appears provides valuable information about the rotational spectroscopy of the polarizable molecule.

An estimation of the molecular polarizability can be obtained from the low-field data using the formula from Ref. [50], which connects $\langle \cos^2\theta \rangle$ to the polarizability anisotropy as:

$$\langle\cos^2\theta\rangle_{J=0} = \frac{1}{3} + \frac{2}{135}\,\Delta\omega$$

$$\langle\cos^2\theta\rangle_{J=1} = \frac{1}{3} + \frac{2}{375}\Delta\omega \tag{1}$$

for H_2 (E,F; ν = 0, J = 0, 1), respectively; where $\Delta\omega = (\alpha_{\parallel} - \alpha_{\perp})\frac{E_o^2}{4B}$, $\alpha_{\parallel,\perp}$the parallel and perpendicular polarizability components, $E_o$the electric field peak value and B the rotational constant. In our experiments involving the E,F state of H_2 (E,F; ν = 0, J = 0) the 532 nm radiation mixes the E,F state with the B and C states of H_2 and the details of this mixed state dictate the difference in polarizability $\alpha_{\parallel} - \alpha_{\perp}$.[17]

IV. Experimental Results and Discussion

A. Non-resonant 532-nm photodissociation of ground state H_2

As shown in Fig. 1, the energy of seven 532 nm photons (16.31 eV) ionizes H_2 molecules (15.43 eV ionization potential) and is enough to produce H_2^+ ν in = 0 - 3. Eight 532-nm photons (18.64 eV) contain enough energy to dissociatively ionize H_2 into H^+. Many nonlinear and perturbative effects in the molecule appear due to the high laser intensities demanded for seven- and eight-photon excitation; producing unique photophysics. Some of the effects observed are above threshold ionization (ATI), ac-Stark shifting of energy levels, shift of the ionization potential, above-threshold dissociation of H_2^+ and excitation of Rydberg states of the neutral molecule.[1, 16, 19, 32]

Fig. 3 presents photoelectron images following the 532-nm ionization of H_2 at two different laser intensities. The intensity profile taken down the middle of the image, along the laser polarization axis, is shown next to each image and shows the H_2^+ ion

yield resulting from the ejection of the electrons at various energies. Photoelectrons with little translational energy from the photoionization process are observed at the center of the image. On average, the more energy the electron receives from the photoionization event the faster it is moving axially and the farther away from the center of the detector it will strike. Several features are observed at these two intensities. Near the center of the image (labeled as 7hν) are photoelectrons originating from the seven-photon ionization of H_2. Seven 532-nm photons have sufficient energy to produce H_2^+ in $\nu = 0 - 3$. Having the lowest available energy, electrons from the formation of H_2^+ ($\nu = 2$ and 3) would be closest to the center of the image that are not observed. However, electrons from $\nu = 0$, and 1 are observed and labeled in Fig. 3 (a and b).

Another feature of the photoelectron images is the blurring of the photoelectrons associated with the seven-photon ionization. As the laser intensity is increased, the blurring affects successively higher energy electrons associated with excitation of lower vibrational levels of H_2^+ ($\nu = 0$ and 1). This blurring effect has been reported before by Chandler and Parker[32] for D_2 photoelectron spectra and Helm et al.[51] for both H_2 and Xe photoelectron spectra. Helm et al. proposed several possible phenomena to explain this effect: non-resonant ionization, tunneling ionization, and double ionization.[51] A mechanism of neutral Rydberg state excitation followed by either field ionization or autoionization producing "zero kinetic energy" or low kinetic energy electrons, respectively, that are subsequently accelerated by the laser beam's ponderomotive potential[33] was later proposed by Chandler and Parker.[32] At high laser field intensities the ground state of the $H_2^+$and the first excited (dissociative) state of the ion become coupled by the laser field, process known as "bond softening".[1, 16, 32] However, a close look at the photofragment images in Fig. 4, slowly moving H^+ along the laser polarization can be observed which could also be due to direct excitation to the repulsive state, dissociative ionization.[52]

At larger radii, eight-photon, above-threshold ionization (ATI) are also observed and labeled as 8hν. The intensity is distributed over many vibrational levels ($\nu = 2$ - 6) also labeled in Fig. 3, where $\nu = 5$ and 6 are the most intense features. These states are observed presumably due to near resonance interaction of the light at the 6 photon energy with the $\nu = 5$ - 7 states of intermediate C state. From inspection of the photoelectron images, the ATI peak changes shape as a function of laser intensity and

has dramatic enhancement for particular vibrational levels at specific laser intensities. At high laser intensity, the ATI peaks shift to higher energy, as lower vibrational levels of H_2^+ are populated.

Similar to Chandler and Parker's[32] observations on D_2, at a similar laser intensity (3.92×10^{13} W/cm^2), $\nu = 0$ at the seven-photon level is observed to be the very weak photoelectron peak compared to $\nu = 5$ at the eight-photon level (see Fig. 3b), in contrast to Yang et al.[19] who reported it to be the most intense photoelectron peak. On the other hand, at 1.59×10^{14} W/cm^2 laser intensity (Fig. 3a), $\nu = 0$ at the seven-photon level is observed to be a strong peak almost as intense as $\nu = 5$ at the eight-photon level in contrast to Zavriyev and Bucksbaum[33] who stated that it got greatly diminished at a laser intensity of 1×10^{14} W/cm^2.

A straight edge is also observed in both sides of the photoelectron images along the laser polarization in Fig. 3. This is not an artifact from our experimental setup or processing analysis. This real feature is actively being investigated.

Fig. 4 shows photofragment images of H^+ recorded from this process using the same apparatus and under the same conditions as the photoelectrons images of Fig. 3. The H_2^+ can absorb 532-nm photons to a repulsive state and dissociate. One- and two-photon dissociation of H_2^+ is observed in Fig. 4 and is labeled as 1hν, and 2hν, respectively. The images show sharp structure and narrow angular distributions for the ejected H^+. The one-photon dissociation shows very prominent peaks assigned to $\nu = 4 - 6$ (taking into account the uncertainty in magnification ratio of the apparatus). At low laser intensity, $\nu = 5$ appears as the largest peak, followed by $\nu = 6$ and as the laser intensity increases $\nu = 4$ appears and gets stronger (as shown in Fig. 4). The dissociation energy shifts to lower vibrational levels with increasing laser intensity indicating bond softening in the H_2. [1, 4, 6]

Additional angular distribution analysis of the rings in the photofragment images (Fig. 4) at different 532 nm laser intensities was performed for each individual H_2^+ vibrational band observed ($\nu = 4 – 6$) and were fitted to a $\cos^n \theta$ distribution where n/2 represents the number of photons absorbed (See SI Fig. 1). The strongly peaked H^+ images from the 1-photon dissociation of the H_2^+ are strongly peaked with a near $\cos^{12}$ angular distribution. This distribution is nearly independent of the vibrational level that dissociates and much narrower than the dissociation of the same levels if the originating state is the H_2(E,F) state (as we show below). We interpret the sharply

peaked angular distribution that is observed to mean that the H^+ is mainly due to laser selection caused by the initial non-resonant 6-photon absorption process needed to reach the excited states of the H_2 molecule; and not due to either adiabatic alignment of the ground state H_2 molecule or selective dissociation of the H_2^+ caused by the angular dependent coupling of the dissociation channels.[1, 3, 13, 32] The narrow $\cos^{12}$ angular distribution in the images reveal the molecular frame photoelectron spectra.

B. 532-nm dissociation following 2-photon excitation of the E,F electronic state of H_2 molecule

The dissociation mechanism that follows the 2-photon excitation into the E,F electronic state can be represented by: H_2 (E,F; ν = 0, J = 0, 1) + (2 × 532 nm photons) = H(N = 0) + H* (N = 3). The inner ring featuring in the image in Fig. 5 is assigned, by conservation of energy, to originate from 2- 532nm photon excitation following dissociation to H(N = 0) + H*(N = 3). The H^+ image also shows intense structure assigned to photoionization of ν = 5 and 6 of H_2^+.

The electronic distribution of any molecule is distorted when the molecule is exposed to an external electric field. This effect is related to the molecular polarizability and results in an induced dipole moment.[15, 50, 53, 54] The polarizability interaction is governed by a $\cos^2\theta$ distribution where θ is the angle between the molecular axis and the field vector.[55] When the field is sufficiently strong, these anisotropic interactions create directional superpositions of the field-free rotational states in which the molecular axis oscillates about the field direction.[50]

Angular distribution analysis of the H^+ formed from the photodissociation of H_2 (E,F; ν = 0, J = 0, 1) state was performed as a function of laser intensity by defining θ = 0 and 180 degrees along the laser polarization axis and θ = 90 and 270 degrees perpendicular to the laser polarization axis and passing through the middle of the inner circle. Signal around an annulus drawn with width, radius, and center previously determined for each image is integrated around the top and bottom halves of the circle. The top and bottom halves were later averaged.

As shown in Fig. 6, the photodissociation of H_2(E,F; ν = 0, J = 0) state shows a strong laser intensity effects. At low intensities, the angular distribution of the H^+ has a significant contribution from a $\sin^2\theta$ component; while at higher laser intensities a predominantly $\cos^2\theta$ distribution is observed whereas in the case of the J=1 state a

strong intensity dependence of the H^+ is not observed (shown in Fig. 7). This phenomenon could be associated to a mixing between the E,F state and the nearby B and C states induced by the laser field (see Theoretical discussions below).

V. Theoretical Results and Discussions

Fig. 8 shows the fitting of the data for H_2(E,F; J = 0, 1) states. By fitting the data to Eq.(1) for the E,F (J = 0) state, as shown in Fig. 8, we find a molecular polarizability of 103 ± 37 a.u., a value that is 93 times smaller than the one given by the literature.[17] This discrepancy is expected, since the theoretical value is estimated taking a static electric field into account. For a laser pulse at 532 nm, the E,F and C electronic states do not couple as strongly as in the static case, and as such the high value of $\alpha_\perp$ (-9600 a.u.[17]) expected for a static field is not produced. It is also worth noting that the calculated polarizability anisotropy values 1.8753 a.u.[56] and ~2.02 a.u.[18] found in the literature for the ground state of H_2 were theoretically obtained assuming a static electric field. Even though the measured polarizability of the H_2(E,F) state is much smaller than the theoretical value in a static field, it is still much larger than the ground state polarizability. We observe the angular distribution at the lowest laser powers at two different voltages for the ion optics associated with the mass spectrometer and see no change in the angular distribution. From this observation we conclude that the low voltages of ~1000 Volts / cm are not responsible for any of the alignement or mixing we observe.

As the pulse energy increases, the intensity peak in the angular distribution gradually switches from perpendicular to parallel to the laser polarization. At intermediate field values, though, the distributions show structure that suggests the existence of an interference term. At these values, a local maximum appears at 90 degrees, which is not expected when only one beta parameter is involved in the data. This maximum is produced by the interference between the field-free rotational states. Therefore, the angular distribution should be expressed using a formula that includes all the transitions that take place with the dissociation.

When molecules are prepared at a particular rotational state $|JKM\rangle$, the angular distribution is given by[22]:

$$I(\theta) = \left[d^J_{KM}(\theta)\right]^2\{1 + \beta_2\, P_2[Cos(\theta)]\} \qquad \ldots(2)$$

where β_2 is the spatial anisotropy parameter, $d^J_{KM}(\theta)$ is a Wigner rotation Matrix and $P_2[Cos(\theta)]$ the associated Legendre Polynomial. Therefore, a formula that would describe the angular distributions of our experiment should be consistent with Eq. (2).

We introduce a phenomenologically derived formula, which fits the angular distribution data. The amplitude of the angular distribution should include two terms, one for the initially prepared rotational state $|000\rangle$ and one for the only allowed state, which will mix with the $|000\rangle$ state via the Stark Effect, using first-order perturbation theory, the $|200\rangle$ state:

$$A(\theta) = \left\{ \left[a_{\|,0}Cos(\theta) + a_{\perp,0}Sin(\theta)\right]d^0_{00}(\theta)\sqrt{(1-c^2)} + \left[a_{\|,2}Cos(\theta) + a_{\perp,2}Sin(\theta)\right]c\, d^2_{00}(\theta)\right\} \quad (3)$$

where $a_{\|,j}, a_{\perp,j}$ the complex amplitudes of parallel and perpendicular transitions and c is a mixing parameter. Thus the angular distribution I(θ) is calculated to be even about the laser linear polarization direction by:

$$I(\theta) = \{|A(\theta)|^2 + |A(\pi-\theta)|^2\}/2 \quad \ldots(4)$$

which then yields:

$$I(\theta) = (1-c^2)\{1+\beta_{2(00)}\, P_2[Cos(\theta)]\} + c^2\{1+\beta_{2(22)}\, P_2[Cos(\theta)]\}[d^2_{00}(\theta)]^2 + 2c\sqrt{(1-c^2)}\,\{1+\beta_{2(02)}\, P_2[Cos(\theta)]\}\, d^2_{00}(\theta) \quad \ldots(5)$$

where $\beta_{2(J)}$are the beta parameters of the angular distribution for each contributing term: $\beta_{2(0)}$ for J = 0; $\beta_{2(2)}$ for J = 2 fragments; and $\beta_{2(02)}$ for the interference between J = 0 and J = 2 fragments. The $\beta_{2(02)}$ interference parameter contains phase information about the dissociation process. Thus, each term corresponds to a particular rotational state or interference between them. For low-field measurements, c should be very small. We note that Eq. (5) reduces to the form of Eq. (2) for c = 0 or 1, and that for small values of c, Eq. (5) agrees with Eq. (1).

Fig. 9 shows the structure of the angular distribution of H^* fragments for $E_o = 10^{12}\frac{W}{cm^2}$. At low fields, the distribution is mostly perpendicular ($\beta_{2(0)} \sim -0.3$), whereas at high fields it becomes mostly parallel ($\beta_{2(2)} \sim 1$). To fit the intermediate field data with the pronounced bump at 90 degrees, another beta parameter is needed, which describes a perpendicular transition: $\beta_{2(02)} \sim 0.4$. A table with the best fitting parameters of angular distribution analysis of the H^+ formed from the photodissociation of H_2 (E,F; ν = 0, J = 0, 1) states at different laser intensities can be found in SI Table 1 while the best fitting profiles are shown in Fig. 8a for the case of E,F (J = 0).

The evolution of the angular distribution versus the electric field for the analysis done on the E,F (J = 0) state is shown in Fig. 10. The interference bump is present in distributions with mixing parameters c from 0.1 to 0.3. For higher fields, the mixing becomes even higher, but saturates at ~0.5. This saturation is attributed to the domination of multi-photon transitions, which trigger photoionization rather than dissociation, thus producing more H_2^+ and less H*. We note that, for the same reason, the mean value of $\cos^2\theta$ also saturates at ~0.55, although the electric field value should give a high-field Δω for the calculated polarizability.

The same analysis of the data for H_2 molecules prepared at the E,F (J = 1) state is done using Eq1. for J = 1 and M = 1, 0, -1 (shown in Fig. 8c). The extracted value of the polarizability anisotropy is 101 ± 30 a.u. This value agrees with the experimental value for the E,F (J = 0) fragments. For J = 1, the angular distribution is predominantly parallel for both low- and high-field ($\beta_2 = 0.2$), and thus no interference bump is present at the data. The photofragment angular distribution again saturates at an intermediate value $\langle \mathrm{Cos}^2(\theta) \rangle = 0.44$. The evolution of the angular distribution versus the electric field for the analysis done on the E,F (J = 1) state.

VI. Conclusions

Utilizing Velocity Mapped Imaging we are able to measure the intensity dependence of the angular distributions of H^+ production channels associated either ionization followed by dissociation of H_2(X) with 532 nm laser light or the dissociation followed by ionization of H_2(E,F; ν = 0, J = 0, 1). By quantification of the angular distributions as a function of laser intensity we learn about the

mechanisms that generate the H^+ as well as measure the molecular polarizability of the E,F state of H_2 for the first time.

Photoelectron images from 532 nm laser radiation ionization of H_2 show that the intense laser fields create ponderomotive shifts in the potential energy surfaces and distort the velocity of the emitted electrons that are produced from 7, 8 and 9 photon ionization. At the 7 photon level one observes a strong blurring of the energy levels associated with production of H_2 in the $\nu = 0$ and 1 vibrational states and a complete loss of defined signal from slower electrons associated with the production of $\nu = 2$ and 3. The 8-photon above-threshold ionization is dominated by production of H_2^+ $\nu = 5$ and 6. These states are observed presumably due to near resonance interaction of the light at the 6 photon energy with the $\nu = 5$ - 7 states of intermediate C state. Photofragment images are strongly peaked with a near $\cos^{12}$ angular distribution. This distribution is nearly independent of vibrational level and implies that the sharply peaked angular distribution that is observed is mainly due to laser selection caused by the initial non-resonant 6 photon absorption process needed to reach the excited states of the H_2 molecule. The images reveal the molecular frame photoelectron spectra. The narrow $\cos^{12}$ angular distribution observed as H_2 is selectively ionized means that these images reveal the molecular frame photoelectron spectra.

The angular distribution analysis of the H^+ formed from the photodissociation of H_2 (E,F; $\nu = 0$, $J = 0$) state shows strong laser intensity effects. At low laser intensity, the angular distribution of the H^+ shows a significant contribution from a $\sin^2\theta$ component, while at higher laser intensities a predominantly $\cos^2\theta$ distribution is observed. In the case of the $J = 1$ state, no change in the distribution shape is observed. By quantifying this data, one can extract the molecular polarizability of H_2(E,F) state when irradiated with 532 nm light to be 103 ± 37 a.u. and 101 ± 30 a.u. for E,F ($J = 0$) and E,F ($J = 1$), respectively. These values are almost 19 times more polarizable than the ground state of H_2 [18, 56] and 96 times less than the ground state of the H_2(E,F) state reported by Komasa[17] and exist due to mixing induced by the laser field between the E,F state and the nearby B and C states in a pulsed laser field.

ACKNOWLEDGMENTS

This material is based on work supported by the U.S. Department of Energy, Office of Basic Energy Sciences, Division of Chemical Sciences. We would like to acknowledge the help of Mr. Mark Jaska for assistance in the laboratory.

References

1. P.H. Bucksbaum, A. Zavriyev, H.G. Muller, D.W. Schumacher, "Softening of the H2+ molecular bond in intense laser fields", Phys Rev Lett, 64, 1883 (1990).

2. T.S. Luk, C.K. Rhodes, "Multiphoton dissociative ionization of molecular deuterium", Physical Review A, 38, 6180 (1988).

3. D. Normand, J. Morellec, "Competition between photoionisation and predissociation of excited states of H2: laser intensity effects", J. Phys. B: At. Mol. Opt. Phys., 21, L625 (1988).

4. J.M. Shull, S. Beckwith, "Interstellar Molecular Hydrogen", Ann. Rev. Astron. Astrophys., 1982, 163 (1982).

5. D. Bailly, E.J. Salumbides, M. Vervloet, W. Ubachs, "Accurate level energies in the EF1, GK1, H1, B1, , B′1, , , J1Δgstates of H2", Molecular Physics, 108, 827 (2010).

6. G.D. Dickenson, E.J. Salumbides, M. Niu, C. Jungen, S.C. Ross, W. Ubachs, "Precision spectroscopy of high rotational states in H2investigated by Doppler-free two-photon laser spectroscopy in theEF 1Σg+–X 1Σg+system", Physical Review A, 86, (2012).

7. J. Liu, D. Sprecher, F.d.r. Merkt, E.J. Salumbides, W. Ubachs, "Determination of the ionization and dissociation energies of H[sub 2] and He[sub 2]", 495 (2012).

8. C.R. Scheper, C.A. de Lange, A. de Lange, E. Reinhold, W. Ubachs, "Dissociation of H in the energy region at the the H(n=1)+H(n=3) dissociation threshold after (1+1') resonance-enhanced two-photon ionization via the B1Su state", Chemical Physics Letters, 312, 131 (1999).

9. T.M. Trivikram, M.L. Niu, P. Wcisło, W. Ubachs, E.J. Salumbides, "Precision measurements and test of molecular theory in highly excited vibrational states of H2 (v = 11)", Applied Physics B, 122, (2016).

10. W. Ubachs, J.C.J. Koelemeij, K.S.K. Eikema, E.J. Salumbides, "Physics beyond the Standard Model from hydrogen spectroscopy", Journal of Molecular Spectroscopy, 320, 1 (2015).

11. M.L. Niu, E.J. Salumbides, G.D. Dickenson, K.S.E. Eikema, W. Ubachs, "Precision spectroscopy of the X1Sg+, v=0-1(J=0-2) rovibrational splittings in H2, HD and D2", Journal of Molecular Spectroscopy, 300, 44 (2014).

12. M.A. Buntine, D.P. Baldwin, D.W. Chandler, "Photodissociation dynamics of doubly excited Rydberg states of molecular hydrogen", The Journal of Chemical Physics, 96, 5843 (1992).

13. D.W. Chandler, L.R. Thorne, "Measured radiative lifetimes for H2 and HD in the E,F 1Σ+g electronic state", The Journal of Chemical Physics, 85, 1733 (1986).

14. J. Förster, Y.V. Vanne, A. Saenz, "Ionization behavior of molecular hydrogen in intense laser fields: Influence of molecular vibration and alignment", Phys. Rev. A, 90, 053424 (2014).

15. L.J. Frasinski, J. Plumridge, J.H. Posthumus, K. Codling, P.F. Taday, E.J. Divall, A.J. Langley, "Counterintuitive alignment of H2(+) in intense femtosecond laser fields", Phys Rev Lett, 86, 2541 (2001).

16. A. Giusti-Suzort, F.H. Miesi, L.F. DiMaurog, E. Charront, B. Yang, "Dynamics of H2+ in intense laser fields", J. Phys. B: At. Mol. Opt. Phys., 28, 309 (1995).

17. J. Komasa, "In Search for the Negative Polarizability States – the State of Hydrogen Molecule", 48, 151 (2005).

18. W. Kolos, L. Wolniewicz, "Polarizability of the Hydrogen Molecule", The Journal of Chemical Physics, 46, 1426 (1967).

19. B. Yang, M. Saeed, L.F. DiMauro, A. Zavriyev, P.H. Bucksbaum, "High-resolution multiphoton ionization and dissociation ofH2andD2molecules in intense laser fields", Physical Review A, 44, R1458 (1991).

20. X. Urbain, B. Fabre, E.M. Staicu-Casagrande, N. de Ruette, V.M. Andrianarijaona, J. Jureta, J.H. Posthumus, A. Saenz, E. Baldit, C. Cornaggia, "Intense-laser-field ionization of molecular hydrogen in the tunneling regime and its effect on the vibrational excitation of H2+", Phys Rev Lett, 92, 163004 (2004).

21. C. Cornaggia, D. Normand, J. Morellec, G. Mainfray, C. Manus, "Resonant multiphoton ionization ofH2via theE,FΣg+1state: Absorption of photons in the ionization continuum", Physical Review A, 34, 207 (1986).

22. S.T. Pratt, P.M. Dehmer, J.L. Dehmer, "Photoionization dynamics of excited molecular states: D2 C 1Πu", The Journal of Chemical Physics, 87, 4423 (1987).

23. M.A. Quesada, A.M.F. Lau, D.H. Parker, D.W. Chandler, "Observation of Autler-Townes splitting in the multiphoton ionization ofH2: Measurement of vibronic transition moments between excited electronic states", Physical Review A, 36, 4107 (1987).

24. A.U. Hazi, C. Derkits, J.N. Bardsley, "Theoretical study of the lowestΣg+1doubly excited state ofH2", Physical Review A, 27, 1751 (1983).

25. E. Xu, A.P. Hickman, R. Kachru, T. Tsuboi, H. Helm, "Photoelectron spectroscopy of vibrationally excitedH2(E,FΣg+1)", Physical Review A, 40, 7031 (1989).

26. E.Y. Xu, T. Tsuboi, R. Kachru, H. Helm, "Four-photon dissociation and ionization of H2", Physical Review A, 36, 5645 (1987).

27. J.H. Posthumus, "The dynamics of small molecules in intense laser fields", Reports on Progress in Physics, 67, 623 (2004).

28. E.E. Marinero, C.T. Rettner, R.N. Zare, "Quantum-State-Specific Detection of Molecular Hydrogen by Three-Photon Ionization", Physical Review Letters, 48, 1323 (1982).

29. S.L. Anderson, G.D. Kubiak, R.N. Zare, "Resonance-enhanced multiphoton ionization of molecular hydrogen via the E,F 1Sg+ state: photoelectron energy and angular distributions", Chem. Phys. Lett., 105, 22 (1984).

30. H. Rudolph, D.L. Lynch, S.N. Dixit, V. McKoy, W.M. Huo, "(2+1) resonant enhanced multiphoton ionization of H2 via the E,F 1Σ+g state", The Journal of Chemical Physics, 86, 1748 (1987).

31. R.L. Farrow, G.O. Sitz, "Coherent anti-Stokes Raman spectroscopy investigation of the anisotropic vibrational transitions of hydrogen", J. Opt. Soc. Am. B, 6, 865 (1989).

32. D.W. Chandler, D.H. Parker, Velocity Mapping of Multiphoton Excited Molecules, in: J.W.a. Sons (Ed.), Advances in Photochemistry, New York, 1999.

33. A. Zavriyev and P. H. Bucksbaum, In “Molecules in Laser Fields”, A. D. Bandrauk, ed., Dekker, New York (1993).

34. G.O. Sitz, "Gas surface interactions studied with state-prepared molecules", Rep. Prog. Phys., 65, 1165 (2002).

35. E. Watts, G.O. Sitz, "State-to-state scattering in a reactive system: H2(v=1,J=1) from Cu(100)", The Journal of Chemical Physics, 114, 4171 (2001).

36. M. Gostein, H. Parhikhteh, G.O. Sitz, "Survival probability of H2(v=1,J=1) scattered from Cu(110)", Phys Rev Lett, 75, 342 (1995).

37. R.L. Farrow, D.W. Chandler, "Raman pump/probe measurements of state-to-state energy transfer rates in the v=1 state of H2", The Journal of Chemical Physics, 89, 1994 (1988).

38. D.W. Chandler, P.L. Houston, "Two-dimensional imaging of state-selected photodissociation products detected by multiphoton ionization", J. Chem. Phys., 87, 1445 (1987).

39. A.T.J.B. Eppink, D.H. Parker, "Velocity map imaging of ions and electrons using electrostatic lenses: Application in photoelectron and photofragment ion imaging of molecular oxygen", Review of Scientific Instruments, 68, 3477 (1997).

40. D. Townsend, M.P. Minitti, A.G. Suits, "Direct current slice imaging", Review of Scientific Instruments, 74, 2530 (2003).

41. A.G. Suits, R.E. Continetti, Imaging in Chemical Dynamics: The State of the Art, 2000, pp. 1.
42. C.R. Gebhardt, T.P. Rakitzis, P.C. Samartzis, V. Ladopoulos, T.N. Kitsopoulos, "Slice imaging: A new approach to ion imaging and velocity mapping", Review of Scientific Instruments, 72, 3848 (2001).

43. A.J.R. Heck, D.W. Chandler, "Imaging Techniques for the Study of Chemical Reaction Dynamics", Annu. Rev. Phys. Chern., 46, 335 (1995).

44. D.J. Hadden, T.M. Messider, J.G. Leng, S.J. Greaves, "Note: Velocity map imaging the scattering plane of gas surface collisions", Rev Sci Instrum, 87, 106104 (2016).

45. D.J. Harding, J. Neugebohren, D.J. Auerbach, T.N. Kitsopoulos, A.M. Wodtke, "Using Ion Imaging to Measure Velocity Distributions in Surface Scattering Experiments", J Phys Chem A, 119, 12255 (2015).

46. M. Reid, S.P. Koehler, "Validation of velocity map imaging conditions over larger areas", Rev Sci Instrum, 84, 044101 (2013).

47. M.N. Ashfold, N.H. Nahler, A.J. Orr-Ewing, O.P. Vieuxmaire, R.L. Toomes, T.N. Kitsopoulos, I.A. Garcia, D.A. Chestakov, S.M. Wu, D.H. Parker, "Imaging the dynamics of gas phase reactions", Phys Chem Chem Phys, 8, 26 (2006).

48. J.J. Lin, J. Zhou, W. Shiu, K. Liu, "Application of time-sliced ion velocity imaging to crossed molecular beam experiments", Review of Scientific Instruments, 74, 2495 (2003).

49. G. Wu, W. Zhang, H. Pan, Q. Shuai, B. Jiang, D. Dai, X. Yang, "A new crossed molecular beam apparatus using time-sliced ion velocity imaging technique", Rev Sci Instrum, 79, 094104 (2008).

50. B. Friedrich, D. Herschbach, "Polarization of Molecules Induced by Intense Nonresonant Laser Fields", J. Phys. Chem, 99, 15686 (1995).

51. H. Helm, N. Bjerre, M.J. Dyer, D.L. Huestis, M. Saeed, "Images of photoelectrons formed in intense laser fields", Phys Rev Lett, 70, 3221 (1993).

52. W.S. Hopkins, S.R. Mackenzie, "Communication: imaging wavefunctions in dissociative photoionization", J Chem Phys, 135, 081104 (2011).

53. S.E. Choi, R.B. Bernstein, "Theory of oriented symmetric-top molecule beams: Precession, degree of orientation, and photofragmentation of rotationally state-selected molecules", The Journal of Chemical Physics, 85, 150 (1986).

54. R.N. Zare, "Photofragment Angular Distributions From Oriented Symmetric-Top Precursor Molecules", Chem. Phys. Lett. , 156, 1 (1989).

55. W.A. Chupka, "Photoionization of molecular Rydberg states: H2, C 1Πu and its doubly excited states", The Journal of Chemical Physics, 87, 1488 (1987).

56. E. Ishiguro, T. Arai, M. Mizushima, M. Kotani, "On the Polarizability of the Hydrogen Molecule", 65, 178 (1951).

Figure Captions.

Fig. 1. Potential energy curves and dissociation limits for the multiphoton dissociation/ionization of H_2 using non-resonant 532 nm photons (green arrows) from H_2 ground state and 532 nm photons following 2-photon excitation of H_2 (E,F; ν = 0, J = 0, 1). The ground electronic state X($^1\Sigma_g$) and E,F($^1\Sigma_g^+$) potential energy curves for H_2 are shown along with the X($^2\Sigma_g^+$) curves for H_2^+ and its vibrational states and the H (N = 0) + H* (N = 3) dissociation limit.

Fig. 2. Schematic diagram of the VMI apparatus (top view).

Fig. 3. Photoelectron images of H_2 taken using 532 nm laser light with an intensity of 1.59×10^{14} W/cm^2 (a) and 3.92×10^{13} W/cm^2 (b). Black arrow indicates the laser polarization.

Fig. 4. Photofragment images of H_2 taken using 532 nm laser light at different intensities.

Fig. 5. Photofragment Image of the ionization and dissociation of H_2 using velocity mapping imaging. The dissociation mechanism follows the 2+1 REMPI of H_2 throughout the E,F electronic state: H_2 (E,F; ν = 0, J = 0, 1) + (2 × 532 nm photons) = H(N = 0) + H* (N = 3) (inner ring). Outer rings correspond to the vibrational states of H_2^+ (ν = 5 - 6) due to ionization of H_2. White arrow indicates the laser polarization.

Fig. 6. Strong alignment effect observed after the angular distribution analysis of the inner ring feature in the photodissociation of H_2 (E,F; ν = 0, J = 0) state at different 532 nm laser intensities (5.12×10^{10} W/cm^2 – 1.59×10^{14} W/cm^2). Black arrow indicates the laser polarization.

Fig. 7. Strong alignment effect observed after the angular distribution analysis of the inner ring feature in the photodissociation of H_2 (E,F; ν = 0, J = 1) state at different 532 nm laser intensities (5.12×10^{10} W/cm^2 – 1.59×10^{14} W/cm^2). Black arrow indicates the laser polarization.

Fig. 8. Experimental and theoretical analysis of the angular distribution of the inner ring feature in the photodissociation of H_2 (E,F; ν = 0, J = 0,1) states at different 532 nm laser intensities. a) Raw data (orange dots) and fitted results (black profile) for the J=0 case. b) $\cos^2\theta$ vs $\Delta\omega$ plot after data for J=0 were fitted to Eq.1. The correct value of the slope is produced by setting $\delta\alpha = 103$ A.U. c) $\cos^2\theta$ vs $\Delta\omega$ plot after data for J=1 were fitted to Eq.1. The correct value of the slope is produced by setting $\delta\alpha = 101$ A.U.

vs

Fig. 9. Pictorial representation of the three different angular terms which produce the structure of the angular distribution of H* fragments for $E_o = 10^{12}\,\frac{W}{cm^2}$

Fig. 10. Evolution of the mixing between the J=0 and J=2 rovibrational states of H_2 versus the electric field. The insets show the angular distributions of the corresponding data points.

Figure 1.

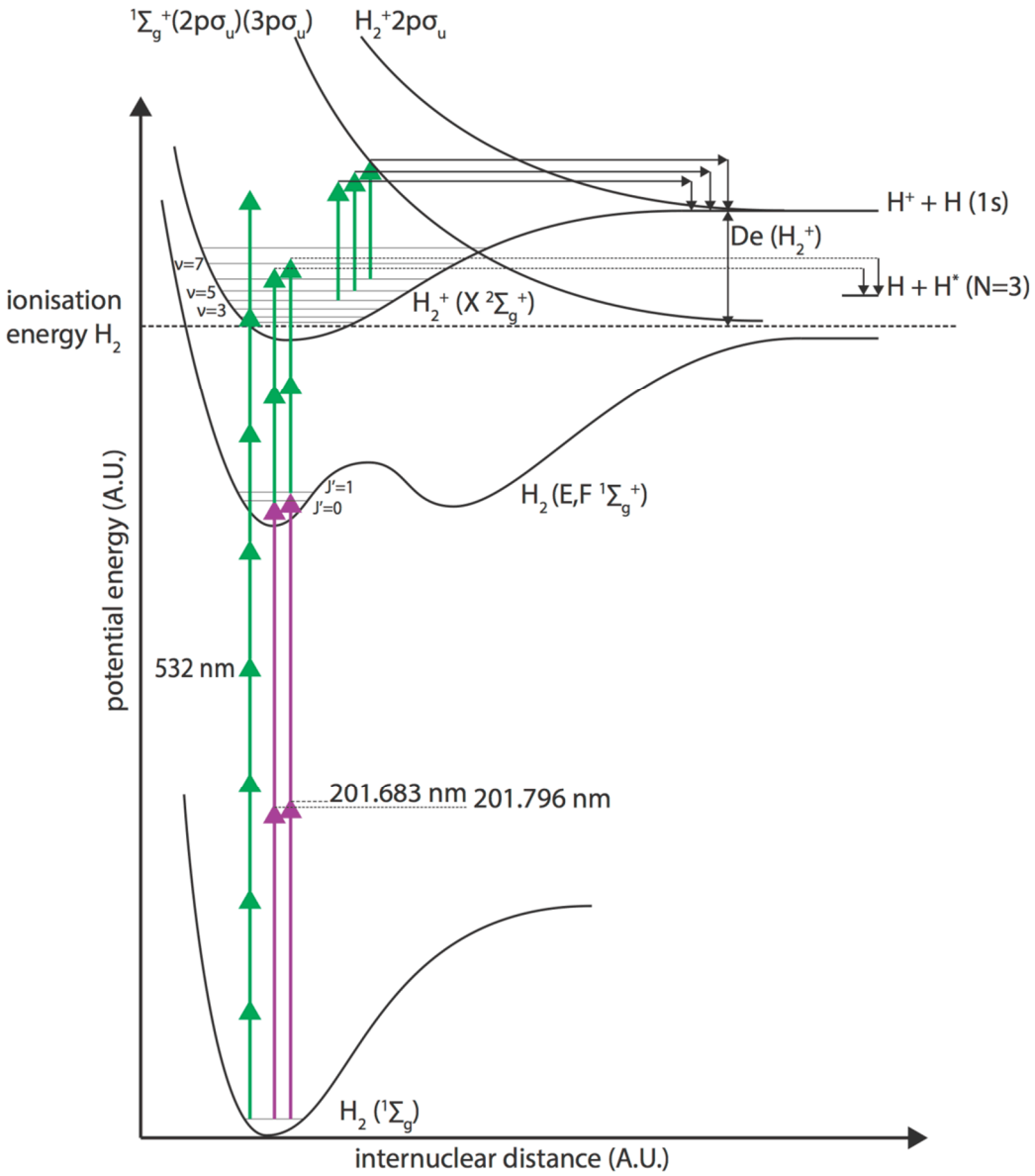
$^1\Sigma_g^+(2p\sigma_u)(3p\sigma_u)$
$H_2^+2p\sigma_u$
$H^+ + H$ (1s)
De (H_2^+)
$H + H^*$ (N=3)
v=7
v=5
v=3
ionisation energy H_2
H_2^+ (X $^2\Sigma_g^+$)
J'=1
J'=0
H_2 (E,F $^1\Sigma_g^+$)
potential energy (A.U.)
532 nm
201.683 nm
201.796 nm
H_2 ($^1\Sigma_g$)
internuclear distance (A.U.)

Figure 2.

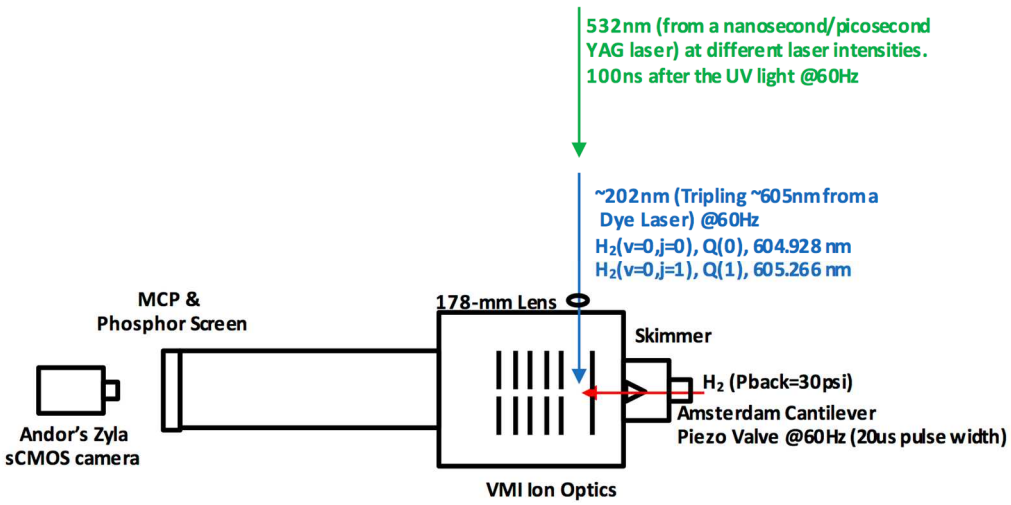
532nm (from a nanosecond/picosecond
YAG laser) at different laser intensities.
100ns after the UV light @60Hz
~202nm (Tripling ~605nm from a
Dye Laser) @60Hz
H2(v=0,j=0), Q(0), 604.928 nm
H2(v=0,j=1), Q(1), 605.266 nm
MCP &
Phosphor Screen
178-mm Lens
Skimmer
H2 (Pback=30psi)
Amsterdam Cantilever
Piezo Valve @60Hz (20us pulse width)
Andor's Zyla
sCMOS camera
VMI Ion Optics

Figure 3.

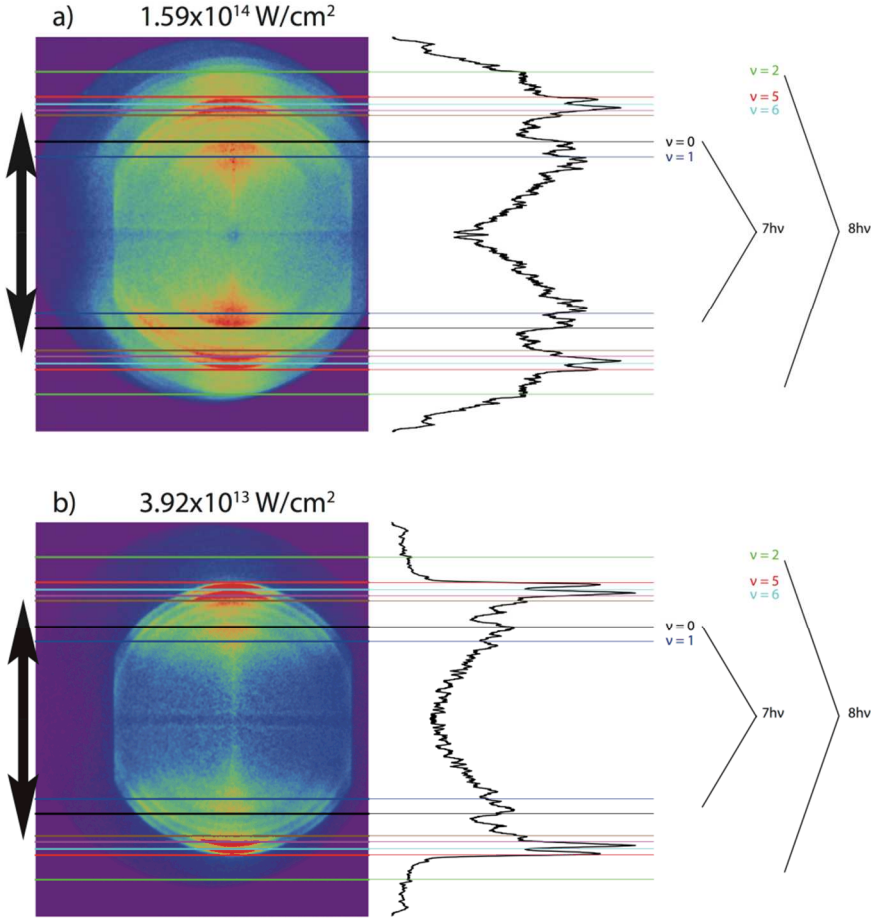
a)
1.59x10^14 W/cm^2
v = 2
v = 5
v = 6
v = 0
v = 1
7hv
8hv
b)
3.92x10^13 W/cm^2
v = 2
v = 5
v = 6
v = 0
v = 1
7hv
8hv

Figure 4.

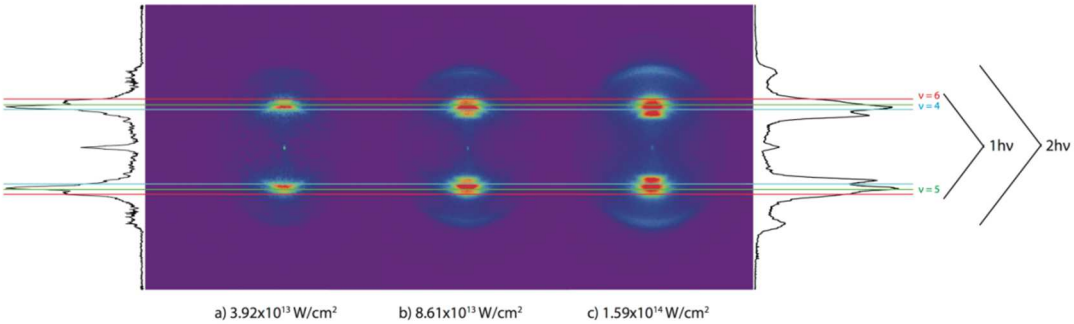
v=6
v=4
v=5
1hv
2hv
a) 3.92x10^13 W/cm^2
b) 8.61x10^13 W/cm^2
c) 1.59x10^14 W/cm^2

Figure 5.

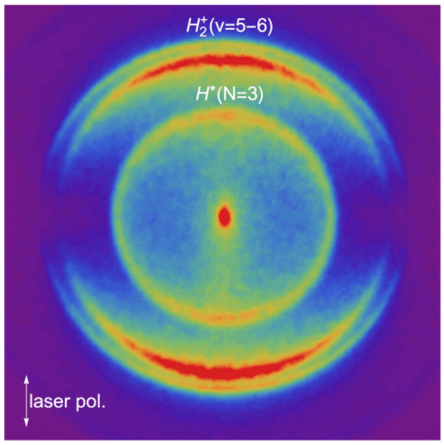

Figure 6.

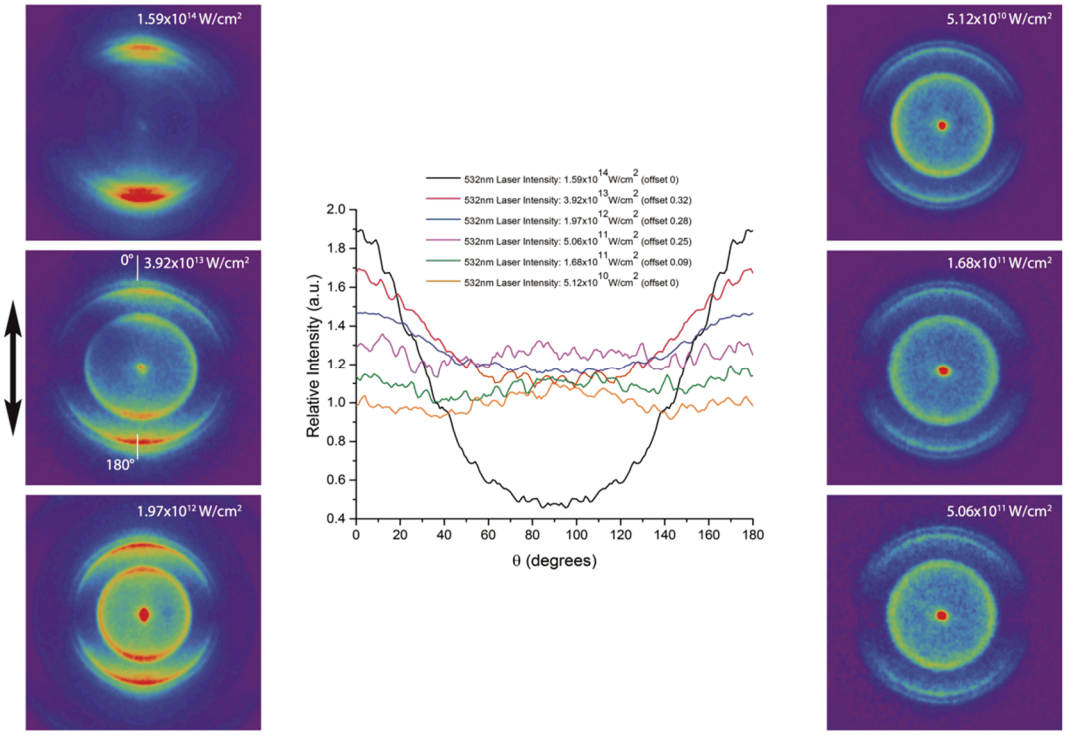
1.59x10¹⁴ W/cm²
0° | 3.92x10¹³ W/cm²
180°
1.97x10¹² W/cm²
532nm Laser Intensity: 1.59x10¹⁴ W/cm² (offset 0)
532nm Laser Intensity: 3.92x10¹³ W/cm² (offset 0.32)
532nm Laser Intensity: 1.97x10¹² W/cm² (offset 0.28)
532nm Laser Intensity: 5.06x10¹¹ W/cm² (offset 0.25)
532nm Laser Intensity: 1.68x10¹¹ W/cm² (offset 0.09)
532nm Laser Intensity: 5.12x10¹⁰ W/cm² (offset 0)
Relative Intensity (a.u.)
θ (degrees)
5.12x10¹⁰ W/cm²
1.68x10¹¹ W/cm²
5.06x10¹¹ W/cm²

Figure 7.

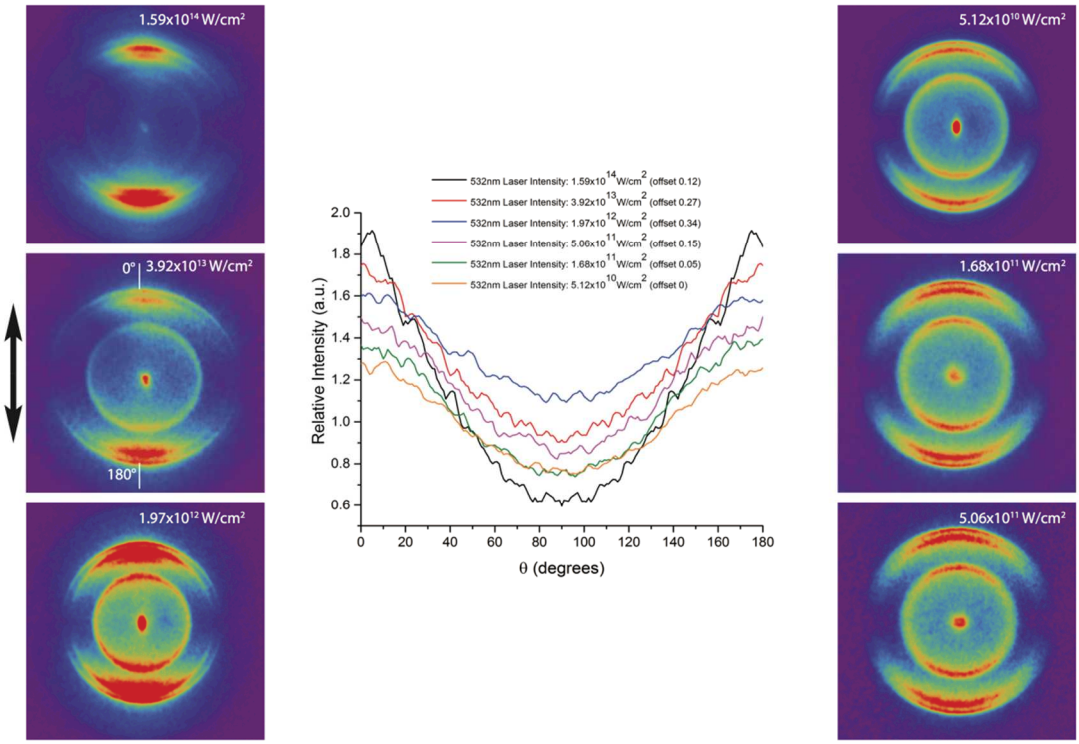
1.59x10¹⁴ W/cm²
0°
3.92x10¹³ W/cm²
180°
1.97x10¹² W/cm²
532nm Laser Intensity: 1.59x10^14 W/cm^2 (offset 0.12)
532nm Laser Intensity: 3.92x10^13 W/cm^2 (offset 0.27)
532nm Laser Intensity: 1.97x10^12 W/cm^2 (offset 0.34)
532nm Laser Intensity: 5.06x10^11 W/cm^2 (offset 0.15)
532nm Laser Intensity: 1.68x10^11 W/cm^2 (offset 0.05)
532nm Laser Intensity: 5.12x10^10 W/cm^2 (offset 0)
Relative Intensity (a.u.)
θ (degrees)
5.12x10¹⁰ W/cm²
1.68x10¹¹ W/cm²
5.06x10¹¹ W/cm²

Figure 8.

a)

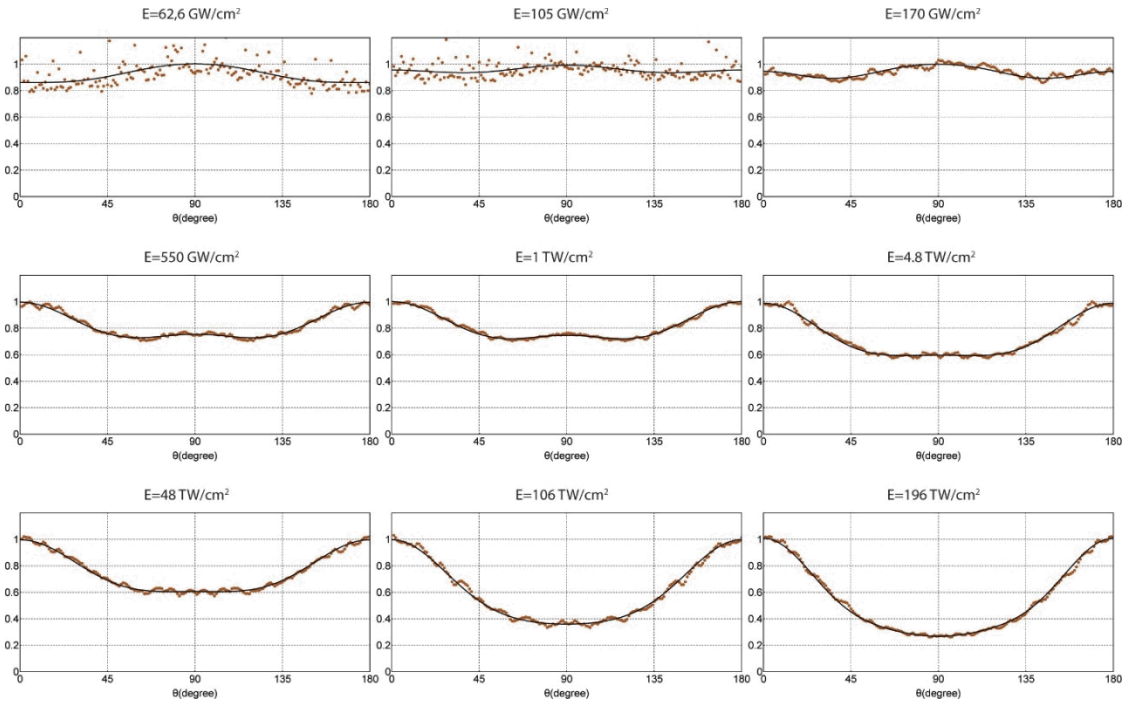
E=62,6 GW/cm²
E=105 GW/cm²
E=170 GW/cm²
E=550 GW/cm²
E=1 TW/cm²
E=4.8 TW/cm²
E=48 TW/cm²
E=106 TW/cm²
E=196 TW/cm²
θ(degree)

b)

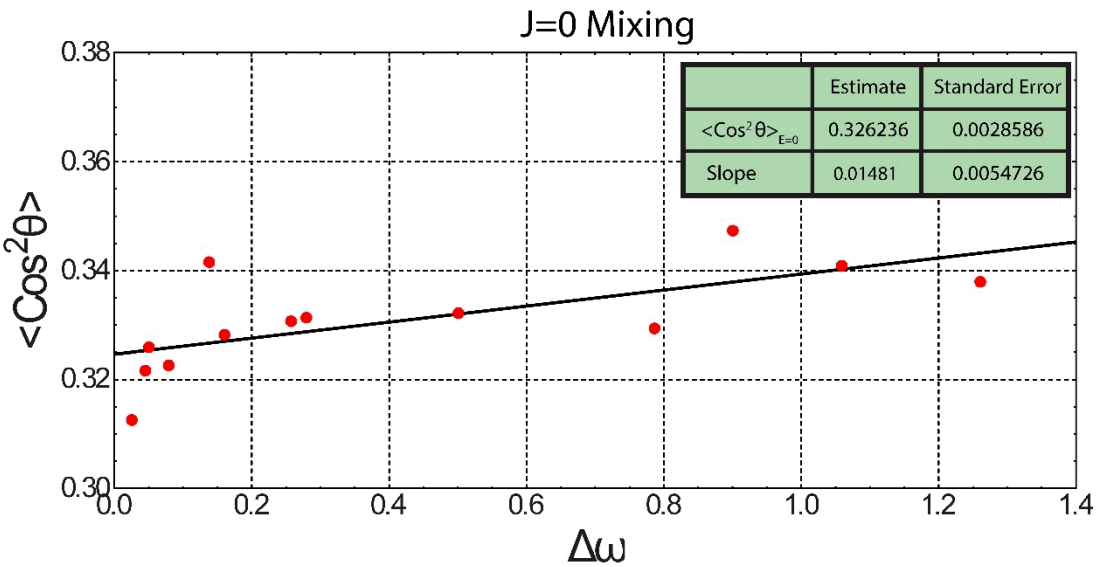
J=0 Mixing
<Cos²θ>
Δω
Estimate
Standard Error
<Cos²θ>E=0
0.326236
0.0028586
Slope
0.01481
0.0054726

Figure 9.

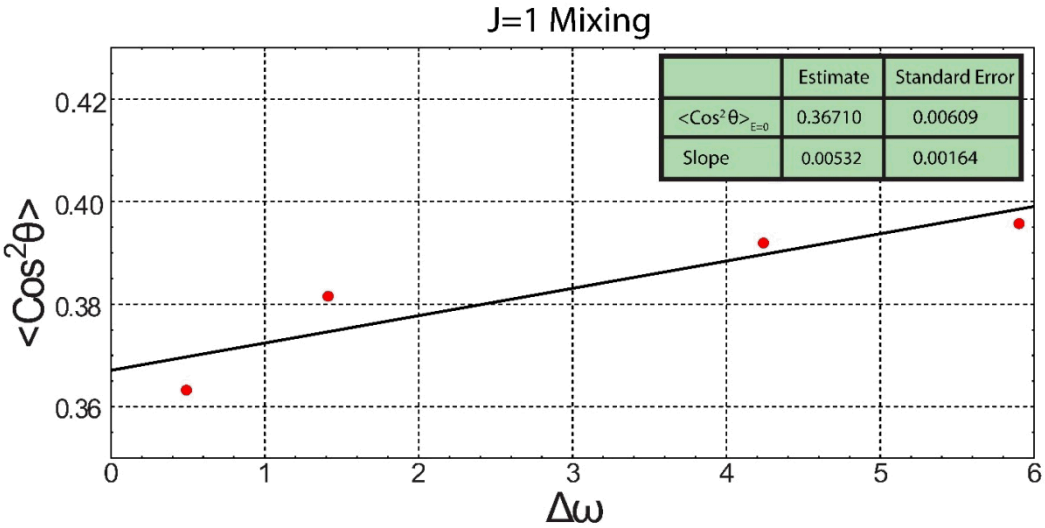
J=1 Mixing
Estimate
Standard Error
<Cos²θ>E=0
0.36710
0.00609
Slope
0.00532
0.00164
0.42
0.40
0.38
0.36
<Cos²θ>
0
1
2
3
4
5
6
Δω

Figure 9

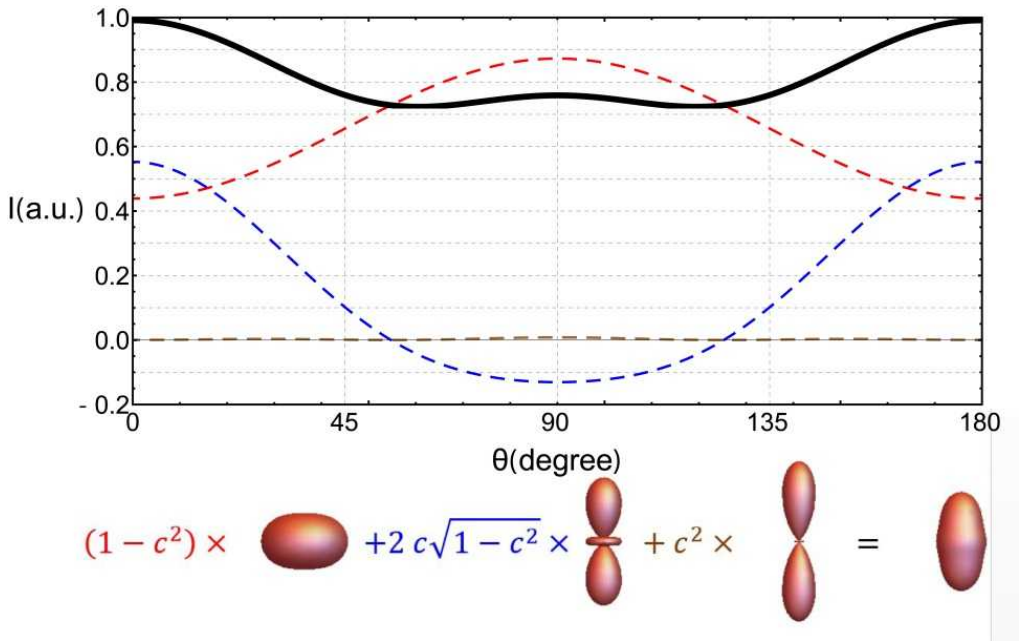
1.0
0.8
0.6
I(a.u.) 0.4
0.2
0.0
- 0.2
0
45
90
135
180
θ(degree)
$(1-c^2)\times$
$+2\,c\sqrt{1-c^2}\times$
$+\,c^2\times$
=

Figure 10.

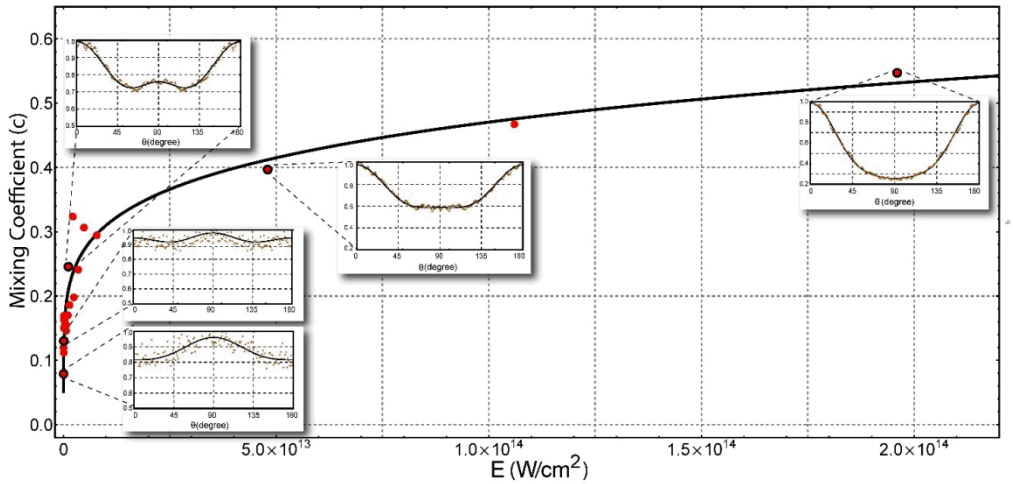
Mixing Coefficient (c)
0.0
0.1
0.2
0.3
0.4
0.5
0.6
0
5.0×10^13
1.0×10^14
1.5×10^14
2.0×10^14
E (W/cm^2)
θ(degree)

Supporting Information:

Multiphoton Ionization and Dissociation of H_2 Molecule in Intense Laser Fields Using Velocity Mapping Imaging

Gary V. Lopez[a], Martin Fournier[a], Justin Jankunas[a], Alexandros K. Spiliotis, T. Peter Rakitzis[b] and David W. Chandler[a]*

[a]*Combustion Research Facility, Sandia National Laboratories, Livermore, California 94550*
[b]*Department of Physics, University of Crete, and Institute of Electronic Structure and Laser, Foundation for Research and Technology-Hellas, Heraklion-Crete,Greece*

*Corresponding Author: chand@sandia.gov

SI. Fig. 1. Additional angular distribution analysis of the rings in the photofragment images in Fig. 5 at different 532 nm laser intensities was performed for each individual H_2^+ vibrational band observed (ν = 4 – 6). The angular distributions were fitted to a $\cos^n \theta$ function where n/2 represents the number of photons absorbed.

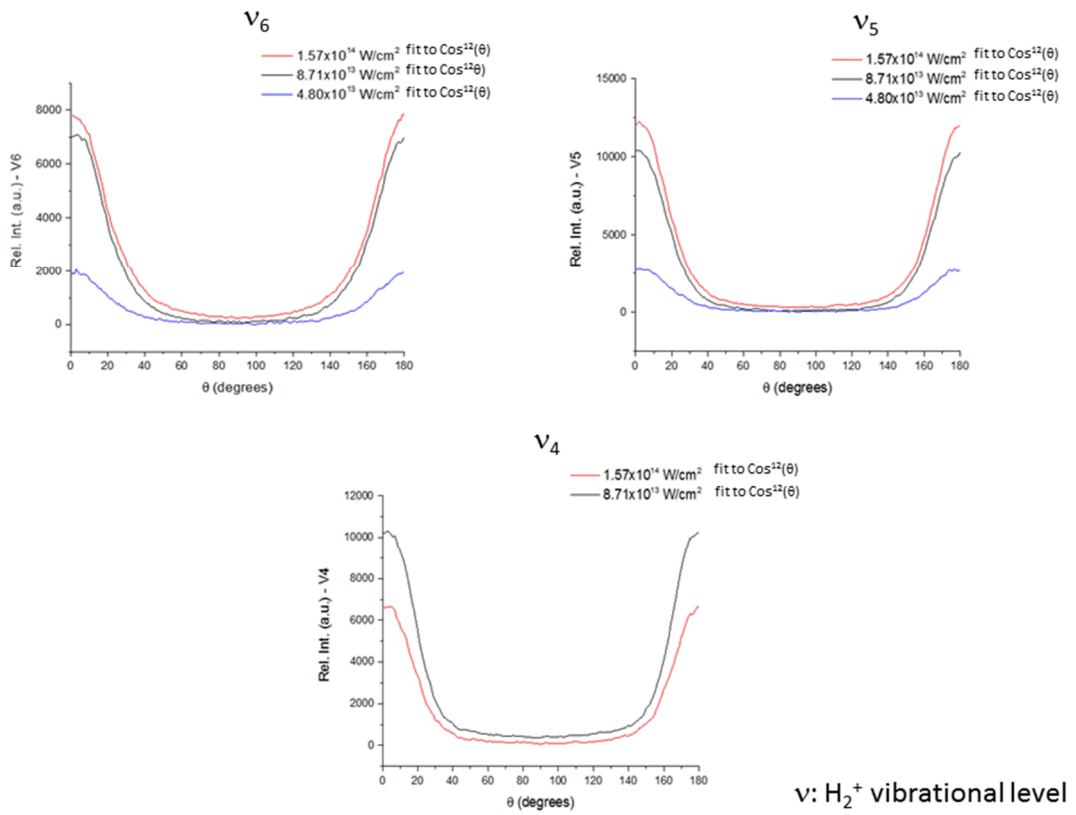

SI. Table 1. Best fit parameters at different laser intensities for J = 0 and 1.

I (GW/cm^2)	c	β2(00)	β2(22)	β2(02)	I (GW/cm^2)	c	β2(00)	β2(22)	β2(02)
15.7	0.0916	-0.3099	1.0137	0.4097	646	0.1459	-0.2903	0.9920	0.3907
30.6	0.06689	-0.3074	1.0036	0.4070	1000	0.1700	-0.3097	1.0103	0.4092
35.8	0.1010	-0.2925	0.9989	0.3977	1150	0.2457	-0.3098	1.0050	0.4098
62.6	0.07798	-0.2901	0.9953	0.3904	1420	0.1863	-0.2902	0.9939	0.3904
105	0.1027	-0.3096	1.0080	0.4095	2420	0.1980	-0.2907	0.9852	0.3902
127	0.1531	-0.3003	1.0002	0.3998	3450	0.2410	-0.3098	0.9989	0.4098
170	0.1047	-0.2902	0.9935	0.3906	4800	0.3065	-0.3096	1.0146	0.4094
204	0.1270	-0.3097	1.0117	0.4093	7840	0.2974	-0.3081	0.9973	0.4078
398	0.1247	-0.3005	0.9996	0.4002	48000	0.3966	-0.2927	0.9932	0.3960
550	0.1659	-0.2920	0.9966	0.3959	106000	0.4671	-0.2902	0.9741	0.3902
624	0.1225	-0.3096	1.0156	0.4091	196000	0.5420	-0.3006	1.0287	0.3934

Appendix A

a. Derivation of $\langle \mathbf{Cos^2(\theta)} \rangle$ vs $\mathbf{\Delta\omega}$

The interaction potential for static polarizability $\delta\alpha = \alpha_{\parallel} - \alpha_{\perp}$ is

$$V_\alpha = -\frac{1}{2} E_o^2 (\delta\alpha \, \mathrm{Cos}^2(\theta) + \alpha_\perp)$$

We employ perturbation theory to include the contribution of this interaction potential to the initial field-free rotational state

$$|00\rangle = |00^{(0)}\rangle + |00^{(1)}\rangle$$

$$\Rightarrow |00^{(1)}\rangle = -\frac{\langle 20|V_\alpha|00\rangle}{E_{J=0} - E_{J=2}} |20^{(0)}\rangle$$

$$= \frac{\Delta\omega}{6} \langle 20|\mathrm{Cos}^2(\theta)|00\rangle \, |20^{(0)}\rangle$$

$$\Rightarrow |00^{(1)}\rangle = \frac{\Delta\omega}{9\sqrt{5}} \, |20^{(0)}\rangle$$

And the state becomes

$$|00\rangle = |00^{(0)}\rangle + \frac{\Delta\omega}{9\sqrt{5}} \, |20^{(0)}\rangle$$

Multiplying both terms with $\cos^2\theta$ and the ket $\langle 00|$ we get

$$\langle \mathrm{Cos}^2(\theta)\rangle = \langle 00^{(0)}|\mathrm{Cos}^2(\theta)|00^{(0)}\rangle + \frac{\Delta\omega}{9\sqrt{5}} \langle 20^{(0)}|\mathrm{Cos}^2(\theta)|00^{(0)}\rangle + \frac{\Delta\omega^2}{405} \langle 20^{(0)}|\mathrm{Cos}^2(\theta)|20^{(0)}\rangle$$

$$\Rightarrow \langle \mathrm{Cos}^2(\theta)\rangle_{\Delta\omega} = \frac{1}{3} + \frac{2}{135}\Delta\omega + \Delta\omega^2 \frac{11}{8505} \quad \ldots (\mathrm{A.}\,1)$$

b. Derivation of $\langle \mathbf{Cos^2(\theta)} \rangle$ vs c

By introducing a mixing parameter c, the normalized coefficients of the perturbation terms become:

$$|00\rangle = \sqrt{(1-c^2)}\left|00^{(0)}\right\rangle + c\left|00^{(1)}\right\rangle$$

$$\Rightarrow \langle \mathrm{Cos}^2(\theta)\rangle = (1-c^2)\left\langle 00^{(0)}\middle|\mathrm{Cos}^2(\theta)\middle|00^{(0)}\right\rangle + 2c\sqrt{(1-c^2)}\left\langle 20^{(0)}\middle|\mathrm{Cos}^2(\theta)\middle|00^{(0)}\right\rangle +$$

$$+ c^2\left\langle 20^{(0)}\middle|\mathrm{Cos}^2(\theta)\middle|20^{(0)}\right\rangle$$

$$\Rightarrow \langle \mathrm{Cos}^2(\theta)\rangle_c = \frac{1}{3}(1-c^2) + \frac{4}{3\sqrt{5}}c\sqrt{(1-c^2)} + \frac{11}{21}c^2 \quad \ldots (\mathrm{A.2})$$

c. Connection between Δω and c

At low field, $c^2 \sim 0$, $\Delta\omega^2 \frac{11}{8505} \sim 0$

So (a.1) and (a.2) become

$$\langle \mathrm{Cos}^2(\theta)\rangle_{\Delta\omega} = \frac{1}{3} + \frac{2}{135}\Delta\omega \qquad (\mathrm{A.3})$$

$$\langle \mathrm{Cos}^2(\theta)\rangle_c = \frac{1}{3} + \frac{4}{3\sqrt{5}}\, c \qquad (\mathrm{A.4})$$

And by equating (A.3) and (A.4) we find

$$c = \frac{4}{161}\Delta\omega \qquad (\mathrm{A.5})$$